Preparation of electrocatalysts by reduction of precursors with sodium citrate†

Stein Trygve Briskeby,[a§] Mikhail Tsypkin,[a‡] Reidar Tunold,[a¶] and Svein Sunde[a,b]

Received Xth XXXXXXXXXX 20XX, Accepted Xth XXXXXXXXX 20XX
First published on the web Xth XXXXXXXXXX 200X
DOI: 10.1039/b000000x

In this work synthesis of Pt/C catalysts by reduction of H_2PtCl_6 with sodium citrate has been investigated. The strong pH–dependence of citrate as a reducing and stabilizing agent has been explored, and an optimum pH range for production of well dispersed catalysts is proposed. To achieve stabilizing and reducing conditions, the presence of both citrate anions and protonated citrates are required. This is achieved in an intermediate pH range between pK_{a2} and pK_{a3} (4.76 and 6.4) of citric acid, where both $C_6H_5O_7^{3-}$ (denoted CA^{3-}) and $C_6H_7O_6^-$ (denoted H_2CA^-) are present. At pH 5.3–5.4 a catalyst with particles around 3 nm was thus successfully prepared. At high pH (∼12) the reduction of Pt is limited, whereas at low pH reduction is fast, but the stabilizing ability of the citrate in solution is poor resulting in large cubic Pt particles. CO-stripping voltammetry indicate that Pt(111) faces are the dominating crystal plane in the nanoparticles formed when citrate anions are used as stabilizing agent. This effect is presumably caused by the distance between oxygen groups in citrate correlating well with the Pt–Pt distance on (111) faces.

1 Introduction

PEM fuel cells have over the last decades proven to be the chosen technology for conversion of chemical energy stored as hydrogen into electrical energy for e.g. vehicle propulsion. A major focus has been on increasing the lifetime of the PEM cells while at the same time reducing the amount of active materials, typically Pt or Pt- containing alloys. From early PEM fuel cell electrodes consisting of PTFE-bonded platinum black applied by hot-press to the ionomeric membrane, substantial reduction in noble metal loading (20–40 times) has been achieved by the introduction of supported catalysts[1]. Typical support materials are carbon blacks like Vulcan XC72 with noble metal loadings ranging from 20–60 wt. % in order to achieve thin active electrode layers minimizing mass transport limitations and ohmic resistance[2,3]. Today's state of the art PEMFC typically have noble metal loadings of 0.05–0.1 mg cm^{-2} [4].

Supported catalysts can be prepared by various methods including ion-exchange, homogenous deposition precipitation (HDP), impregnation and deposition of colloidal particles.[5,6] The former two methods are limited to low loading catalysts[2]. High loadings are readily achieved by impregnation. However, it is challenging to achieve high loading and simultaneously maintain high dispersion of Pt.[7].

Colloidal methods have proven able to achieve both loading and dispersion. Here, the noble metal precursor is chemically reduced in the presence of a protective agent. A narrow particle size distribution is achieved by stabilization of the nanoparticles by either steric hindrance or electrostatic charges. Common protecting ligands include NR_4^+, triphenylphosphine (PPh_3), polyvinylpyrrolidone (PVP) and polyvinyl alcohol (PVA). One drawback with such methods, however, is the presence of the protective agents which can reduce the catalytic function of the nanoparticles. Removal of such agents can be done by washing in appropriate solvents or by thermal decomposition in inert atmosphere[5]. Routes which can omit additional stabilizers would be favourable, though. Such methods include the polyol method, where reduction and stabilization are achieved with ethylene glycol[8–11].

Citric acid is well known for its dual functions as a reducing and stabilizing agent, and was used by Turkevich in the preparation of Pt nanoparticles in 1986[12]. Since then several researchers have used citrate stabilized methods. Gou et al.[13,14] prepared Pt/C and PtRu/C electrocatalysts by reduction of chloroplatinic acid and ruthenium chloride with sodium borohydrate. Citrate was used as stabilizing agent in ammonium hydroxide solutions of pH 11–13. The ratio citrate:noble metal was varied, and optimum ratios of 2:1 and 1:1

† Electronic Supplementary Information (ESI) available: [details of any supplementary information available should be included here]. See DOI: 10.1039/b000000x/

[a] *Department of Materials Science and Engineering, Norwegian University of Science and Technology (NTNU), NO-7491 Trondheim, Norway.*
[b] *Fax: +47 7359 1105; Tel: +47 7359 4051; E-mail: svein.sunde@ntnu.no*
§ Present address: Statoil ASA, Herøya Forskningspark, Hydroveien 67, 3936 Porsgrunn, Norway
‡ Present address: NEL Hydrogen AS, Heddalsvegen 11, 3674 Notodden, Norway
¶ Professor Reidar Tunold, 1933 – 2013

were found for Pt/C and PtRu/C respectively [13,14]. Xu et al. [15] prepared bimetallic PtRu/C catalysts by a similar approach and found that the resulting particle size changed when the stabilizing pH varied between 5 and 13. At a pH of 7, homogenous catalysts were achieved. A citrate-stabilized method with different reducing agents ($NaBH_4$ and formaldehyde) and carbon support was studied by Jiang et al. [16]. In the studies above, the catalysts were prepared by methods in which citrate only acted as stabilizer. Incomplete reduction of Pt, leaving Pt of higher valences in the catalysts due to complex formation with citrate anions, has been thought to make additional reducing agents necessary. In studies by Henglein [17,18] the formation of carbonyls upon exposing colloids prepared by reduction and stabilization with citrate to CO revealed that traces of unreduced Pt were present at the colloid surface. These results were confirmed by EXAFS studies by Lin et al. [19].

In this study Pt/C electrocatalysts with a nominal Pt-loading of 10 wt. % were prepared by a citrate method in which citrate anions act both as reducing and stabilizing agent. The stabilizing and reducing abilities of citrate at varying pH are discussed, and an optimum pH for synthesis of highly dispersed catalysts is proposed.

2 Experimental

Platinum colloids were prepared by reduction of chloroplatinic acid ($H_2PtCl_6 \cdot 6H_2O$, VWR) with tri-sodium citrate ($C_6H_5Na_3O_7 \cdot 2H_2O$, sds). 37 ml MilliQ water and 2 ml of a $H_2PtCl_6 \cdot 6H_2O$ prepared by dissolving 1 g of $H_2PtCl_6 \cdot 6H_2O$ in 50 ml water were heated to boiling in a three-necked round bottle flask equipped with a reflux tube. The reaction mixture was de-aerated by purging of Ar through a Pasteur pipette. The third neck was used for collecting samples of the reaction mixture. When the solution reached the boiling point, 11 ml of a 1 % tri-sodium citrate solution was added. After mixing, aliquots of the boiling reaction mixture were collected every 5 minutes and quenched in an ice bath. These samples were later used for preparation of samples for UV-vis measurements. The pH of the solution was measured before and after the reaction was quenched. (This synthesis will be referred to as "medium pH" or "intermediate pH" below.)

The synthesis was repeated at low and high pH by replacing 1 ml of water with 1 ml of 1 M HCl or 2 ml of water by 2 ml 1 M NaOH respectively. (The samples were denoted "Low pH" and "High pH" respectively.) A list of experimental parameters can be found in Table 1.

Platinum reduction was studied by UV-vis spectrophotometry using a Cary 5 UV-Vis-NIR spectrophotometer. UV-vis samples were prepared by diluting 1 part of reaction mixture with 7 parts of MilliQ water. As reference, a diluted solution containing water and tri-sodium citrate of the same concentration as the colloids was used. This blank sample was subjected to the same treatment as the colloids. UV-vis absorption spectra were recorded between 500 and 190 nm with a scan rate of 150 nm/min.

Electrocatalysts with a nominal loading of 10 wt. % Pt were prepared by addition of Vulcan XC-72 carbon (Cabot) during different stages of the colloid formation and at medium and low pH, giving catalysts with different particle size. After catalyst synthesis, the catalyst was separated from the solution by filtration (Millipore DVPP filter 0.65 μm) and washed thoroughly with MilliQ water, until neutral pH was achieved in the washing water.

Transmission Electron Microscopy images were recorded of both colloidal samples and catalysts by means of a JEOL 2010F electron microscope equipped with a field emission gun. The Pt loading was determined by Energy Dispersive Spectroscopy in a Hitachi S-3500N low vacuum SEM with an Oxford EDS Detector. (The acceleration voltage was 15 kV, and the working distance 10 mm.) XRD was carried out using a D8-focus X-ray diffractometer with Cu Kα radiation.

The catalysts were characterized electrochemically using thin-film electrodes applied to the 5 mm glassy carbon disk of a rotating ring-disk electrode (Pine Instrument Company). Prior to electrode preparation, the disk was polished to a mirror finish with 0.05 μm alumina solution (Buehler). Electrodes were prepared by a procedure described by Schmidt et al. [20] and Paulus et al. [21], in which 20 μl of a slurry with known catalyst content was pipetted on to a rotating disk electrode. The composition of the ink used in this study was 1 mg catalyst per 1 ml of a 20 % isopropanol in water solution. The electrode was placed under argon during drying. When the electrode was completely dry, 20 μl of a Nafion solution (Alfa Aesar 5 % w/w) diluted 1:100 with water, was applied to the electrode. After evaporation of the solvent, a Nafion film of approximately 0.1 μm was formed, binding the catalyst to the glassy carbon surface.

Electrochemical characterization was performed in 0.5 M sulphuric acid (Merck, p.a.) in a three electrode setup with a reversible hydrogen reference electrode. A Pt wire, contained in a glass tube separated from the working electrolyte by a glass frit acted as counter electrode. The electrode was cycled between 50 mV and 1.4 V at a scan rate of 100 mV/s. The electrolyte was saturated with oxygen. The fifteenth cycle was recorded.

CO-stripping voltammetry was performed between 50 and 1100 mV vs. RHE at a sweep rate of 100 mV s^{-1} after adsorbing CO at 220 mV. Before adsorption of CO the electrode was cycled at 100 mV/s between 50 and 1100 mV vs. RHE in a deaerated 0.5 M H_2SO_4 electrolyte until a stable voltammogram was recorded. Prior to CO-stripping, excess CO was removed from the electrolyte by flushing with Ar for 30 min.

Table 1 Experimental parameters. pH was measured using a pH electrode (Radiometer PHM210) which was calibrated with buffers of pH 7.000 and 4.005 (Radiometer analytical) on a daily basis. The concentrations of H_2PtCl_6 solutions were 0.0386 M in all solutions. All citrate-containing solutions contained 1 wt. % $C_6H_5Na_3O_7 \cdot 2\,H_2O$.

Sample	Chemicals	pH_{start}	pH_{end}	Reaction time /minutes
Low pH	2 ml H_2PtCl_6 solution 11 ml $C_6H_5Na_3O_7 \cdot 2\,H_2O$ solution 36 ml H_2O 1ml 1 M HCl	2.26	2.28	80
Medium pH	2 ml H_2PtCl_6 solution 11 ml $C_6H_5Na_3O_7 \cdot 2\,H_2O$ solution 37 ml H_2O	5.53	5.28	80
High pH	2 ml H_2PtCl_6 solution 11 ml $C_6H_5Na_3O_7 \cdot 2\,H_2O$ solution 35 ml H_2O 2ml 1 M NaOH	12.29	12.19	80
PtC-L	100 mg XC-72 2 ml H_2PtCl_6 solution 11 ml $C_6H_5Na_3O_7 \cdot 2\,H_2O$ solution 36 ml H_2O 1ml 1 M HCl	2.54	2,2	80
PtC-N	100 mg XC-72 2 ml H_2PtCl_6 solution 11 ml $C_6H_5Na_3O_7 \cdot 2\,H_2O$ solution 37 ml H_2O	5.52	5.23	80

3 Results

Fig. 1 shows UV-vis absorption spectra recorded at different times during reduction of $PtCl_6^{2-}$ at intermediate pH. Before the reaction started, a clearly discernible peak at 260 nm corresponding to Pt^{IV} as the complex $PtCl_6^{2-}$ was observed. This peak diminished with time, and had completely disappeared after 25 min when the reduction was complete.

A plot showing concentration of $PtCl_6^{2-}$ vs. time for the reduction reaction at different pH is given in Fig. 2. Concentrations were calculated from the height of the absorption peak at 260 nm in the UV-Vis absorption spectra. The absorption measured in the last aliquot (after 80 min of reaction) was taken as a $PtCl_6^{2-}$ concentration of zero. In the case of reduction at high pH the Pt absorption peak did not disappear during the experiment. The absorption curve recorded at low pH at the end of the reaction was used as a reference to convert the absorption data to concentration. During the course of reaction a shift in colour from pale yellow to dark brown/black was observed at low and intermediate pH. At high pH, no colour change occurred.

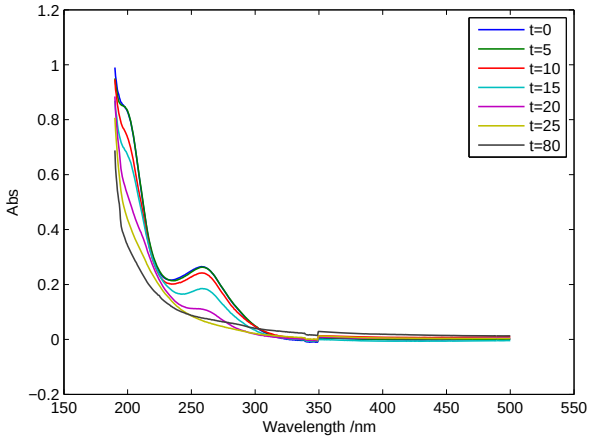

Fig. 1 UV-vis absorption data from colloid synthesis at intermediate pH. The peak at 260 nm disappearing with time is related to absorption by $PtCl_6^{2-}$. The initial concentration of $PtCl_6^{2-}$ was 0.001544 M which was further diluted adding seven parts of MilliQ water to one part of the $PtCl_6^{2-}$ solution.

Fig. 3 shows TEM images of the colloids prepared at low and intermediate pH. Since Pt reduction was limited at high pH, TEM was not attempted for this experiment. (A TEM sample prepared with this solution would in practice be an impregnation of the TEM grid with a solution containing a Pt salt, and not be representative of any particles formed at reaction conditions.) At low pH the particles are around 10 nm of size and have a well–defined cubic shape. At intermediate pH a "worm"– like shape with a diameter of around 2 nm was

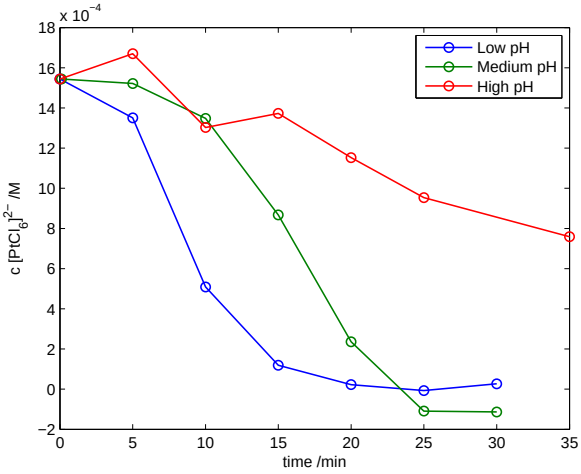

Fig. 2 Effect of pH on reduction of H_2PtCl_6 The rate of reduction increases as pH during synthesis is lowered.

observed. We believe that this shape is an artifact originating from the drying of the TEM samples, however. During sample preparation, the TEM grid is wetted by colloid solution. As water evaporates the Pt particles agglomerate forming the shapes in Fig. 3(b).

Fig. 4 shows catalysts prepared at intermediate pH with carbon addition before (Fig. 4(a)) and after (Fig. 4(b)) colloid formation. As seen from the figure, carbon needs to be added at the beginning of the reduction to give a well dispersed catalyst. Adding carbon after colloid formation yields a catalyst with a high degree of agglomeration.

TEM images of catalysts prepared at low and intermediate pH are given in Fig. 5. Virtually no Pt was deposited when catalyst preparation was attempted at high pH, and data are hence not included. Large Pt particles and the same cubic shape as was seen in the STEM images of the colloids (Fig. 3) are seen for the catalyst prepared at low pH. (Average particle size, based on TEM images is presented along with other data below.)

Fig. 6(a) and 6(c) display cyclic voltammograms of the catalysts prepared at low and intermediate pH respectively. The voltammograms were recorded in oxygen–saturated electrolyte during oxygen reduction experiments. (The oxygen in the electrolyte explains the negative offset in the voltammograms originating from reduction of oxygen.) The electrochemical surface area (ESA) of the catalysts was calculated from the hydrogen desorption charge between 50 and 400 mV after subtracting the double layer charge. ESA for the catalyst prepared at low and intermediate pH was found to be 4 $m^2\ g^{-1}$ Pt and 93 $m^2\ g^{-1}$ Pt respectively, resulting in particle sizes of 67 and 3 nm assuming spherical monodisperse particles. The uncertainty in the calculations for the low–pH cata-

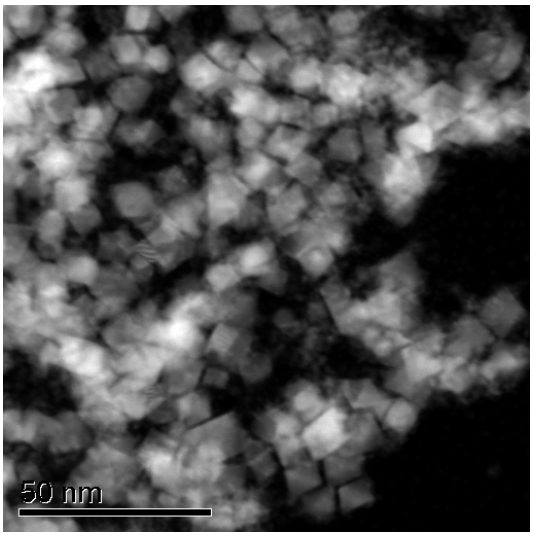

(a)

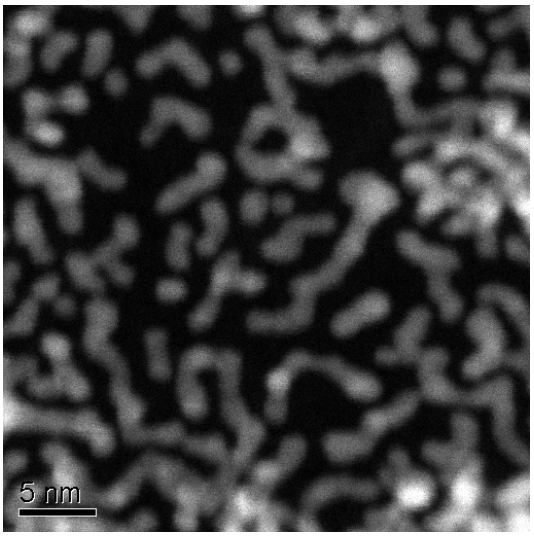

(b)

Fig. 3 STEM images of colloids prepared at low (a) and intermediate (b) pH during colloid formation.

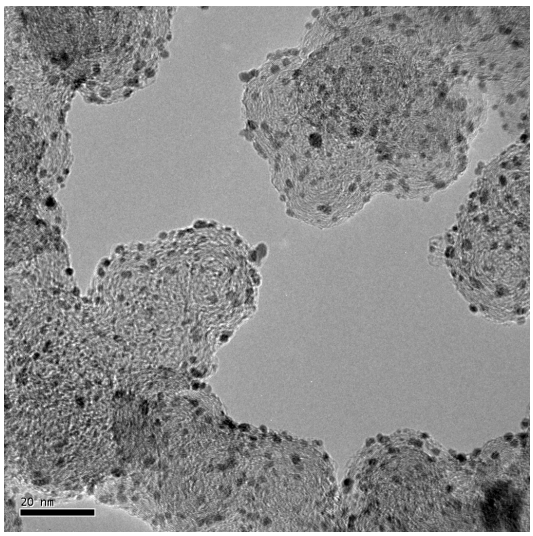

(a)

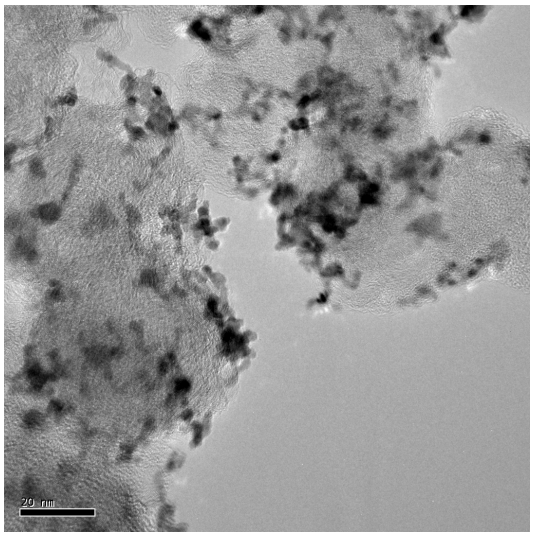

(b)

Fig. 4 TEM images of catalysts prepared by adding carbon before (a) and after (b) colloid formation. Catalyst and colloid synthesis was performed at medium pH.

lyst is high as the electrochemical response is small compared to the double–layer charging and oxygen reduction currents.

Fig. 6(b) and 6(d) show CO-stripping voltammograms for the two catalysts. For both catalysts, two stripping peaks appear at 0.79 and 0.89 V. The dominant peak for the catalyst prepared at low pH is the low potential peak, and for the catalyst prepared at intermediate pH the higher potential peak dominates completely. The differences indicate that changes in synthesis parameters induce different surfaces on the Pt particles.

Based on the hydrogen desorption and CO-stripping charge, ESA was calculated subtracting the background from the first sweep in the case of H_{UPD} and second scan for CO-stripping. The hydrogen UPD charge was integrated between 50 and 420 mV for both catalysts, whereas the CO-stripping charge was integrated from 600 mV or 720 mV for PtC-L and PtC-N respectively. The upper vertex potential was used as the upper integration limit. ESA for the different calculations are given in Table 2 along with loading and estimates of particle size.

The XRD data for catalysts prepared at low and intermediate pH are, given in Fig. 7, and were refined using Bruker AXS Topas v2.1 refinement software. The background was

Table 2 Loading and electrochemical surface area of the catalysts calculated by a) hydrogen desorption charge from Fig. 6; b) hydrogen desorption charge from CO-stripping voltammograms in Fig. 6; c) CO-stripping charge from voltammograms in Fig. 6. The corresponding particle diameter d are included along with estimates of particle diameter from TEM and XRD.

Catalyst	Loading	ESA /m^2 g^{-1} Pt			Particle size, d /nm				
	/wt. %	a	b	c	a	b	c	TEM	XRD
PtC-N	13	93.2	104.1	91.6	3.0	2.7	3.1	2.3	4.6
PtC-L	11	4.2	15.8	18.1	66.8	17.7	15.5	181	24.7

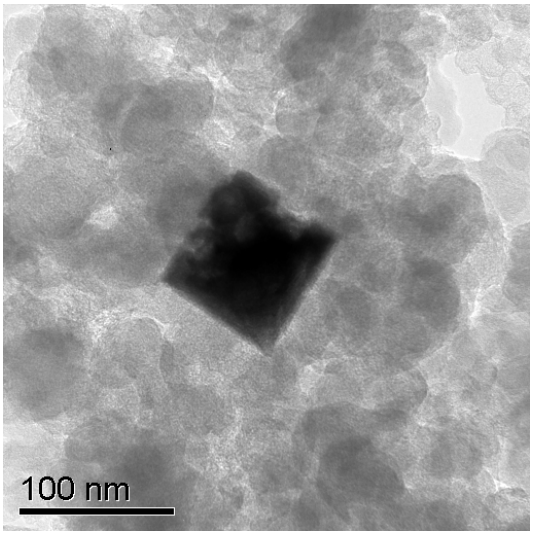

(a)

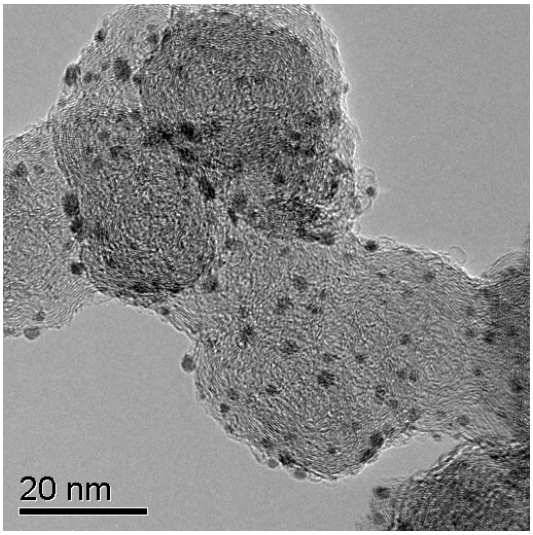

(b)

Fig. 5 TEM images of catalysts prepared at low (a) and medium pH (b).

modeled using a Chebyshev polynomial and whole-powder pattern fitting was used for analysis of the powder structural parameters. The resulting average crystallite size are reported in Table 2. In the figure, broader peaks are observed in the case of PtC-N compared to PtC-L, in line with the difference in particle size for the two catalysts. For PtC-L a substantially larger size is estimated from the TEM images than from the diffractograms, though.

The electrochemical measurements clearly display the difference in active surface area between the catalysts. For PtC-L the electrochemical response from Pt is small compared to the carbon background. The small area makes the active surface area calculations inaccurate. This is apparent in Table 2 where the calculated surface areas and corresponding particle sizes show considerable variation. The discrepancy between the average size from TEM images and the electrochemical surface area of PtC-L can be explained by difference in measuring technique. Electrochemically, all active area is measured, whereas for TEM, a 2D projection of particles and agglomerates forms the basis for calculation. For PtC-N all measurements are relatively consistent, although modelling of XRD-spectra for catalysts with particle sizes approaching 3 nm can be questioned.

The difference in size estimated from the TEM images and the diffractograms for sample PtC-L, Table 2, is presumably due to the agglomeration in the catalyst synthesized at this pH. XRD measures crystallite size, whereas TEM would give particle size. Indications of agglomeration in sample PtC-L were in fact observed in a number of the TEM images (not shown) for this sample.

4 Discussion

The combined effect of pH on concentration of reducing and stabilizing species can be explained by the degree of protonation of citrate anions. Hence, the reduction of $PtCl_6^{2-}$ by citrate is strongly dependent on pH. As seen from Fig. 2, the reduction rate increases with decreasing pH, indicating that protonated citrate species are needed for the reduction to take place. At high pH ($\sim$12) complete reduction was not achieved during the experiments. Lin et al.[19] and Pron'kin et al.[22] proposed the overall reactions for citrate reduction of Pt in Eq. (1)

and (2) respectively *.

$$PtCl_6^{2-} + H_2CA^- + H_2O \longrightarrow Pt^0 + CO_2 + H^+ + Cl^- \quad (1)$$

$$9\,PtCl_6^{2-} + 2\,H_2CA^- + 10\,H_2O \longrightarrow 9\,Pt^0 + 12\,CO_2 + 38\,H^+ + 54\,Cl^- \quad (2)$$

In Fig. 8 a log(c) - pH plot of the triprotic citric acid with pK_a values of 3.13, 4.76 and 6.4 is displayed[23,24]. In the case of high pH, protonated citrates are almost absent, hence little or no reduction is expected. As pH is lowered protonation occurs and the concentration of the lower-valent citrate anions increase. At the intermediate pH (5.3–5.5) in these experiments HCA^{2-} and H_2CA^- are the two dominating species, and an increased rate of reduction is observed. A further decrease of the pH (2.2–2.5) results in a further increase in reaction rate although the concentration of the assumed reducing agent, H_2CA^-, according to Fig. 8, is approximately unchanged. This result suggests that the participation of H_3CA in the reduction cannot be excluded, although not being included in Equations (1) and (2).

The stabilizing effect of tridendate oxoanion stabilizers, like citrate ($C_6H_5O_7^{3-}$), are believed to be caused by the good match between the ligand O−O and surface M−M distances. The citrate anion with O−O distances between 2.8–3.1 Å matches well with the interatomic distance of Pt of 2.77 Å, c. f. Fig. 4 of Ref.[25]. As seen from the TEMs for both the colloids and catalysts prepared at intermediate and low pH (Figures 3 and 5) the particle size increases considerably as pH, and consequently the concentration of CA^{3-}, is decreased. Based on these results, an optimum pH region for the formation of small Pt particles with narrow particle size distributions would lie in an intermediate pH range between pK_{a2} and pK_{a3} (4.76 and 6.4) where both CA^{3-} and H_2CA^- are present.

The differences seen in TEM pictures of the colloid (Fig. 3 (b)) compared to the catalyst (Fig. 5(b)) prepared under similar conditions are believed to be caused by TEM sample preparation. In Fig. 3 (b), extended Pt domains are seen. These are not found in the catalyst. Similar structures have also been reported by others[26]. These authors pointed out that Pt agglomeration occurred during sample preparation of Pt on glassy carbon (GC) electrodes by wet chemical deposition due to supersaturation of the GC surface by H_2PtCl_6 precursor. In our case, a colloidal Pt solution was dropped onto a carbon coated TEM grid. The colloidal solution is likely to contain Pt of higher valences in the form of $PtCl_6^{2-}$ or in citrate complexes. Guo et al.[13] and Henglein[17] have observed Pt of higher valence state when using the citrate stabilized synthesis methods. Guo prepared Pt/C electrocatalysts by reduction of chloroplatinic acid with sodium borohydrate with citric acid as stabilizing agent in ammonium hydroxide solution at CA:Pt ratios of 1:1, 2:1, 3:1, 4:1. XPS measurements revealed relatively higher amount of Pt in metallic state for the latter three ratios. Henglein observed Pt of higher valence when colloids formed by reduction of chloroplatinic acid with sodium citrate were subjected to CO by bubbling resulting in the formation of carbonyl complexes of the form$[Pt_3(CO)_6]_n^{2-}$ with n = 1 to ∼10. The complexes were not formed if the colloid had been subjected to hydrogen bubbling before CO bubbling. The agglomeration in our case can thus be explained by the presence of higher valence Pt, either on the surface of the colloidal particles or in solution. When water is evaporated during TEM sample preparation, supersaturation is obtained, leading to agglomeration as was also described by Maillard et al.[26] for electrode preparation by wet chemical deposition from H_2PtCl_4 precursors. The same kind of agglomeration would not be that pronounced in TEM images of colloids prepared at low pH (Fig. 3 (a)) as the particles are considerably larger.

For electrocatalyst preparation, we expect the presence of higher valence Pt in the catalyst to have few practical implications, as reduction and oxidation of platinum takes place when the potential of a catalyst coated electrode is cycled.

Adding carbon at the beginning of the synthesis is necessary for achieving well dispersed catalysts with the current synthesis method. As seen from Fig. 4, agglomeration occurs when carbon is added after colloid formation. When carbon is present from the beginning, ion exchange with Pt can take place before the reduction starts, forming favourable nucleation centers on the carbon surface. This is not achieved when the colloid is already formed.

At low pH, the size of synthesized particles is very sensitive to small changes in pH. Comparing the TEM of the supported catalyst prepared at low pH (Fig. 5(a)) and the colloid formed at low pH (Fig. 3 (a)), considerable difference in particle size is observed. At low pH, the concentration of $C_6H_5O_7^{3-}$ is nearly negligible, but it changes to a power of 3 with respect to pH. Hence, even very small differences in pH will have large impact on the concentration of stabilizer and can greatly effect the resulting particle size. The carbon and interactions with the precursor could also affect the final particle size. When synthesis is performed at low pH, little control with particle size is expected.

The electrochemical measurements displays features in line with the Pt crystal structure which is expected for catalysts prepared by a citrate stabilized synthesis. Platinum has a face-centered cubic structure (FCC). For Pt particles a cubo-octahedral structure with eight octahedral (111) crystal faces and six cubic (100) crystal faces is preferred, as a minimum surface energy is obtained[27,28]. The TEM images of the col-

* Note that the equations are not correctly balanced. In Eq. (2) the number of protons on the right side should be 34 to keep mass and charge balance.

loid and catalyst prepared at low pH (Figures 3 (a) and 5(a)) show cubic particles. In the presence of citrate stabilizer it is reasonable to assume that the (111) crystal phase of Pt is energetically preferred, as the Pt-Pt distance matches the O-O distance in citrate as discussed above. For (100) the Pt-Pt distances of 3.92 and 2.77 Å are found, whereas for (111) the Pt-Pt distance is 2.77 Å. Hence, catalysts prepared at a pH where the concentration of CA^{3-} is high should be dominated by (111) faces as this crystal plane is stabilized by citrate. In the voltammograms of Fig. 6 the main CO-stripping peak recorded on PtC-N is located at 0.89 V. A small shoulder is located at 0.79 V. For PtC-L, the main stripping peak is found at the lower potential (0.79 V) with a second peak at the higher potential. Work on single crystal surfaces of Pt(100) and Pt(111) has shown peak separations in this order of magnitude between the different faces, and with CO-stripping from Pt(111) taking place at the highest potential[29–32]. Qualitatively these results indicate that nanoparticles formed at intermediate pH in this work have faces predominantly of Pt(111), very much in line with what is expected from citrate stabilization. The effect of edges and steps, which should constitute a relatively large fraction of surface atoms for small nanoparticles, may, however, also contribute to shifts in the stripping potential[33] as well as do the presence of agglomerates[34,35], the assessment of which both are beyond the scope of the present work.

5 Conclusion

The strong pH–dependence of citrate as a reducing and stabilizing agent has been explored, and an optimum pH range for the production of well dispersed catalysts is proposed. To achieve stabilizing and reducing conditions, both citrate anions and protonated citrates are needed. This is achieved in an intermediate pH range between pK_{a2} and pK_{a3} (4.76 and 6.4) of citric acid, where both CA^{3-} and H_2CA^- are present. At pH 5.3–5.4 a catalyst with particles around 3 nm was thus successfully prepared. At high pH ($\sim$12) the reduction of Pt is limited, whereas at low pH reduction is fast, but the stabilizing ability of the citrate in solution is poor resulting in large Pt particles.

CO-stripping voltammograms show that Pt(111) faces are the dominating crystal plane in the nanoparticles formed when citrate anions are used as stabilizing agent. This effect is presumably caused by the distance between oxygen groups in citrate correlating well with the Pt–Pt distance on (111) faces.

Acknowledgments

Work at NTNU was supported by The Norwegian Research Council through the NANOMAT program, contract no 158516/S10 and the EU project FURIM (6th EU Framework Programme, contract no. SES6-CT-2004-502782). John Walmsley from SINTEF, Materials and Chemistry is acknowledged for assistance with TEM data collection.

References

1 S. Gottesfeld and T. A. Zawodzinski, in *Advances in Electrochemical Science and Engineering*, ed. R. C. Alkire, H. Gerischer, D. M. Kolb and C. W. Tobias, Wiley-VCH Verlag GmbH, 2008, vol. 5, ch. 4, pp. 195–301.
2 I. Kvande, S. T. Briskeby, M. Tsypkin, M. Rønning, S. Sunde, R. Tunold and D. Chen, *Top. Catal.*, 2007, **45**, 81–85.
3 J. Lee, K. Han, S. Park, H. Kim and H. Kim, *Electrochim. Acta*, 2004, **50**, 807–810.
4 Y. Zhou, K. Neyerlin, T. S. Olson, S. Pylypenko, J. Bult, H. N. Dinh, T. Gennett, Z. Shao and R. O'Hayre, *Energy Environ. Sci.*, 2010, **3**, 1437–1446.
5 K. Chan, J. Ding, J. Ren, S. Cheng and K. Tsang, *J Mater Chem*, 2004, **14**, 505–516.
6 M. Toebes, M. van der Lee, L. Tang, M. H. in't Veld, J. Bitter, A. van Dillen and K. de Jong, *J. Phys. Chem. B*, 2004, **108**, 11611–11619.
7 Z. Zhou, S. Wang, W. Zhou, G. Wang, L. Jiang, W. Li, S. Song, J. Liu, G. Sun and Q. Xin, *Chem. Commun.*, 2003, 394–395.
8 Y. Wang, J. Ren, K. Deng, L. Gui and Y. Tang, *Chemistry of Materials*, 2000, **12**, 1622–1627.
9 F. Bonet, V. Delmas, S. Grugeon, R. Urbina, P. Silvert and K. Tekaia-Elhsissen, *Nanostruct Mater*, 1999, **11**, 1277–1284.
10 F. Bonet, K. Tekaia-Elhsissen and K. Sarathy, *Bull Mat Sci*, 2000, **23**, 165–168.
11 Z. Zhou, W. Zhou, S. Wang, G. Wang, L. Jiang, H. Li, G. Sun and Q. Xin, *Catal Today*, 2004, **93-95**, 523–528.
12 J. Turkevich, R. Miner and L. Babenkova, *J. Phys. Chem.*, 1986, **90**, 4765–4767.
13 J. Guo, T. Zhao, J. Prabhuram and C. Wong, *Electrochim. Acta*, 2005, **50**, 1973–1983.
14 J. Guo, T. Zhao, J. Prabhuram, R. Chen and C. Wong, *Electrochim. Acta*, 2005, **51**, 754–763.
15 Y. Xu, X. Xie, J. Guo, S. Wang, Y. Wang and V. Mathur, *J. Power Sources*, 2006, **162**, 132–140.
16 Q. lai Jiang, Z. dong Peng, X. feng Xie, K. Du, G. rong Hu and Y. xiang Liu, *Transactions of Nonferrous Metals Society of China*, 2011, **21**, 127 – 132.
17 F. Henglein, *J Phys Chem B*, 1997, **101**, 5889–5894.
18 A. Henglein and M. Giersig, *J Phys Chem B*, 2000, **104**, 6767–6772.
19 C.-S. Lin, M. R. Khan and S. D. Lin, *Journal of Colloid and Interface Science*, 2005, **287**, 366 – 369.
20 T. Schmidt, H. Gasteiger, G. Stab, P. Urban, D. Kolb and R. Behm, *J. Electrochem. Soc.*, 1998, **145**, 2354–2358.
21 U. Paulus, T. Schmidt, H. Gasteiger and R. Behm, *J. Electroanal. Chem.*, 2001, **495**, 134–145.
22 S. Pron'kin, G. Tsirlina, O. Petrii and S. Vassiliev, *Electrochimica Acta*, 2001, **46**, 2343 – 2351.
23 *CRC Handbook of Chemistry and Physics*, ed. D. R. Lide, CRC Press, 88th edn., 2007-2008, pp. 8–46.
24 *The Merck Index*, ed. S. Budavari, Meck Research Laboratories, 12th edn., 1996.
25 R. Finke and S. Özkar, *Coord. Chem. Rev.*, 2004, **248**, 135–146.
26 F. Maillard, S. Schreier, M. Hanzlik, E. R. Savinova, S. Weinkauf and U. Stimming, *Phys. Chem. Chem. Phys.*, 2005, **7**, 385–393.
27 K. Kinoshita, *J. Electrochem. Soc.*, 1990, **137**, 845–848.

28 W. Romanowski, *Surface Science*, 1969, **18**, 373 – 388.
29 P. Inkaew, W. Zhou and C. Korzeniewski, *J. Electroanal. Chem.*, 2008, **614**, 93 – 100.
30 E. Herrero, B. Álvarez, J. M. Feliu, S. Blais, Z. Radovic-Hrapovic and G. Jerkiewicz, *J. Electroanal. Chem.*, 2004, **567**, 139 – 149.
31 N. Lebedeva, M. Koper, E. Herrero, J. Feliu and R. van Santen, *J. Electroanal. Chem.*, 2000, **487**, 37 – 44.
32 N. P. Lebedeva, M. T. Koper, J. M. Feliu and R. A. van Santen, *Electrochemistry Communications*, 2000, **2**, 487 – 490.
33 J. M. Feliú, E. Herrero and V. Climent, in *Catalysis in Electrochemistry*, ed. E. Santos and W. Schmickler, John Wiley & Sons, Inc., 2011, pp. 127–163.
34 F. Maillard, S. Schreier, M. Hanzlik, E. R. Savinova, S. Weinkauf and U. Stimming, *Phys. Chem. Chem. Phys.*, 2005, **7**, 385 – 393.
35 A. López-Cudero, J. Solla-Gullón, E. Herrero, A. Aldaz and J. M. Feliú, *J. Electroanal. Chem.*, 2010, **644**, 117 – 126.

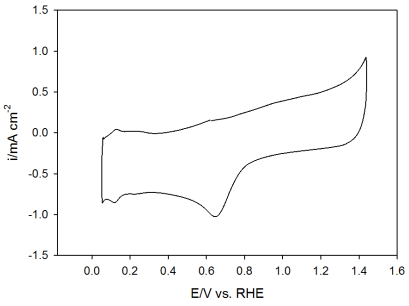

(a)

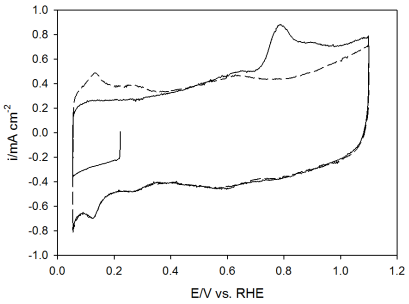

(b)

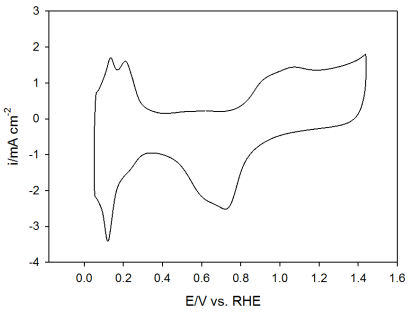

(c)

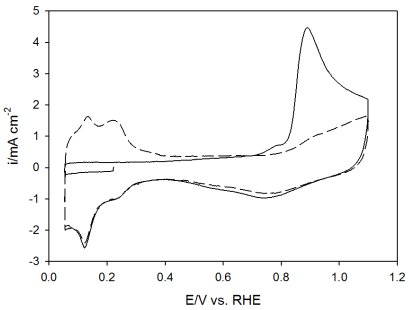

(d)

Fig. 6 Cyclic voltammograms of catalysts prepared by reduction with sodium citrate at low (a) and intermediate (c) pH. CO-stripping voltammograms (solid line) of catalysts prepared by reduction with sodium citrate at low (b) and intermediate (d) pH. For the two latter the consecutive CV is included (dashed line).

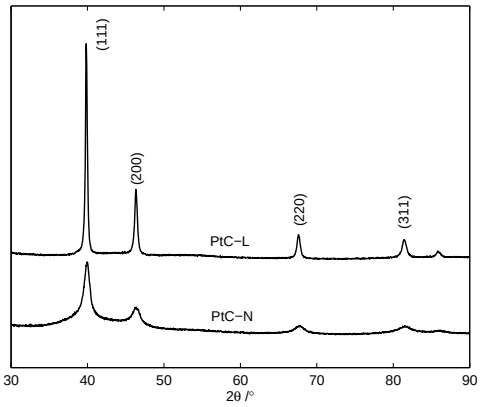

Fig. 7 XRD of catalysts prepared at low and intermediate pH.

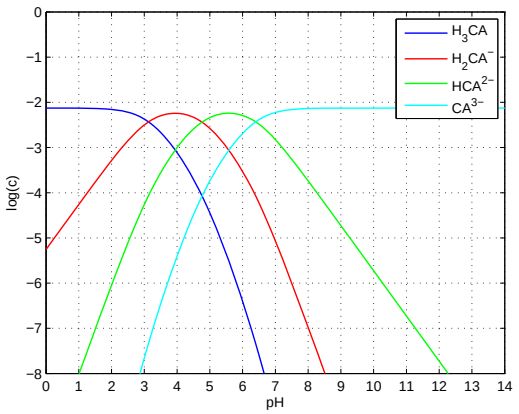

Fig. 8 Calculated log(c)-pH plot for citric acid. (pK_a values of 3.13, 4.76 and 6.4 [23,24].)